Anal. Bioanal. Electrochem., Vol. 11, No. 1, 2019, 59-69

Analytical & Bioanalytical Electrochemistry

www.abechem.com

Full Paper

High Performance Nano Sponge $Li_{1.2}Mn_{0.54}Ni_{0.13}Co_{0.13}O_2$ Cathode via Synthesizing Nano Plate Precursor for Lithium Ion Battery

Mohadese Rastgoo-Deylami,[1,2] Mehran Javanbakht,[1,2,*] and Hamid Omidvar[2, 3]

[1]*Department of Chemistry, Amirkabir University of Technology, Tehran, 1599637111, Iran*
[2]*Renewable Energy Research Center, Amirkabir University of Technology, Tehran, 1599637111, Iran*
[3]*Department of Mining and Metallurgical Engineering, Amirkabir University of Technology, Tehran, 1599637111, Iran*

[*]Corresponding Author, Tel.: +982164545806 ; Fax: +982164545781
E-Mail: mehranjavanbakht@gmail.com

Received: 15 September 2018 / Accepted with minor revision: 10 January 2019 / Published online: 31 January 2019

Abstract- In this work, we synthesized nano plate oxalate precursor via solvothermal method to obtain Nano Sponge $Li_{1.2}Mn_{0.54}Ni_{0.13}Co_{0.13}O_2$ (NS-LMNCO) cathode material. During solvothemal process, ethanol and water solvents arrange oxalate nuclei to form plate-like shape. With increasing temperature at calcination step, the oxalate precursor is converted to NS-LMNCO by removing CO_2. The structure, morphology and elemental composition of synthesized samples are investigated with X-ray diffraction (XRD), Scanning Electron Microscopy (SEM), Transmission Electron Microscopy (TEM) and X-ray Photoelectron spectroscopy (XPS), respectively. The thickness and length of nano plate are 60 nm and 2 µm, respectively. However, the diameter of particles made NS-LMNCO is 40 nm. The NS-LMNCO delivers discharge capacities of 207.6 mAh g^{-1} at 0.1 C. Furthermore, electrochemical data show that NS-LMNCO sample retain discharge capacities of 147.5 mAh g^{-1} (71.1% of the first discharge capacity) after 50 cycles at 0.1 C-rate. The results obtained in this work clearly confirmed that electrochemical properties of lithium ion cell e.g. specific capacity, cycle life and rate performance can be significantly controlled by properties of active materials, especially cathode particles, e.g. porosity, surface area and density related to morphology of active particles.

Keywords- Hydrothermal/solvothermal synthesis, Oxalate precursor, Lithium rich cathode materials, Nano Sponge $Li_{1.2}Mn_{0.54}Ni_{0.13}Co_{0.13}O_2$, Lithium ion battery

1. INTRODUCTION

A development of Energy Storage Systems (ESSs) storing renewable energies can significantly prevent global warming arising from burning fossil fuels. Hence, in the current century, many researchers focus on the designing high performance ESSs, especially high energy density battery. Lithium-ion Battery (LIB) fabricated by Sony Co in 1991 is one of the most important rechargeable batteries can store electrical energy with lithium ion diffusion in structure of cathode and anode materials during charge and discharge process. A LIB includes remarkable electrochemical properties e.g. high power density, high output voltage and high cycle life controlled by structural properties of electrode materials, especially cathode particles [1].

So far, a large numbers of cathode materials with different structure are presented for LIB such as $LiCoO_2$ (Layered) [2], $LiMn_2O_4$ (Spinel) [3], $LiFePO_4$ (Olivine) [4, 5], $LiMn_xNi_yCo_{1-x-y}O_2$ (Layered) [6] and lithium rich (xLi_2MnO_3. (1-x) $LiMO_2$(M=Ni, Mn, Co, Fe, etc. Layered-Layered) [7]. In Li-rich $Li_{1.2}Mn_{0.54}Ni_{0.13}Co_{0.13}O_2$ cathode material, the x value is equal of 0.5. This cathode is consisted of two layered components, Li_2MnO_3 and $LiMn_{1/3}Co_{1/3}Ni_{1/3}O_2$. This cathode theoretically exhibits capacity of 377 mAh g^{-1} at potential range of 2-4.8 V versus lithium. It should be noticed that the Li_2MnO_3 component leads to stabilized structure and an increase capacity of lithium rich material [8]. However, the $Li_{1.2}Mn_{0.54}Ni_{0.13}Co_{0.13}O_2$ shows some disadvantages e.g. low initial coulombic efficiency, low rate capability and low cycle life. In order to overcoming mentioned problems, different methods such as designing morphology of particles [9], doping metal elements in layered structure of Li-rich material [10] and coating surface of Li-rich particles [8] are applied.

A morphology of cathode particles can be significantly controlled with applying different synthesis procedures. Several approaches have been conducted for obtaining $Li_{1.2}Mn_{0.54}Ni_{0.13}Co_{0.13}O_2$ cathode material: Hydrothermal/ Solvothermal synthesis [9], precipitation method [10, 11], solid-state reaction [12] and freeze drying [11]. Most important parameters effected on electrochemical performance e.g. size and shape of particles, purity and phase crystallinity of materials highly depend on synthetic route. For example, different morphology of materials can be prepared with changing reaction temperature, precipitant agent, reaction time and solvent in hydro/ solvothermal synthesis. Since crystal and nuclei growth rates and assembling of formed nuclei in autoclave can be changed by the mentioned parameters. Furthermore, compared to other synthesis methods, hydro/ solvothermal method is easy and controllable procedure.

In recent years, some important electrode materials are produced and their electrochemical properties are improved by our researchers [13-17]. In this study, we present the structure-controlled solvothermal method of Nano plate oxalate precursor to obtain 3D architectures of $Li_{1.2}Mn_{0.54}Ni_{0.13}Co_{0.13}O_2$ with good structural and electrochemical properties. The nuclei arrangement in autoclave, size and morphology of oxalate precursor can be controlled by

solvent type. In procedure mentioned here, ethanol with deionized water leads to prepared good solvent system to obtain nano structure of oxalate precursor.

The structure and morphology of the oxalate precursor and Li-rich particles are evaluated by using Field Emission Scanning Electron Microscopy (FE-SEM), Transmission Electron Microscopy (TEM) and an X-ray diffraction (XRD). Finally, the electrodes of Li-rich particles are fabricated and their electrochemical performances are investigated as the cathode electrode in Li-ion cell. The electrochemical results confirmed that the NS-LMNCO shows good electrochemical performance in Li-ion cell.

2. EXPERIMENTAL

2.1. Preparation of the samples

The Nano plate oxalate precursor had been synthesized via hydro/ solvothermal reaction from $Li(CH_3COO).2H_2O$, $Ni(CH_3COO)_2.4H_2O$, $Mn(CH_3COO)_2.4H_2O$ and $Co(CH_3COO)_2.4H_2O$ with oxalic acid as precipitant agent. First, stoichiometric amount of all mentioned acetate salts are dissolved in deionized water and ethanol (V: V= 1:2) under stirring for 45 minutes. It should be noticed that the 5% atomic excess of Lithium source is added since lithium can be evaporated at high temperature at calcination step. Then, the appropriate amount of oxalic acid is added to above solution. Afterwards, it is moved to a 100 mL autoclave. It should be noticed that the autoclave is made of two chambers. The Teflon chamber is located inside of stainless steel chamber. The autoclave is heated at 180 ºC for 18 h by hot silicon oil bath. During Hydro/ Solvothermal reaction, the oxalate nuclei are obtained in autoclave. After cooling down autoclave, the precipitates are separated by filtration, washed with alcohol, ethanol, and heated at 85 ºC overnight for obtaining dried powders. Finally, the oxalate precursor is calcinated at 250 ºC for 2 h, 500 ºC for 6 h and 850 ºC for 6 h in the air to prepare NS-LMNCO powder.

2.2. Characterization

The X-ray diffraction (XRD) using an Equinox 3000 with Cu Kα radiation (λ=0.15418 nm) is used to investigate a crystallinity of the prepared samples. Furthermore, field emission scanning electrode microscopy (FE-SEM) and Transmission Electron microscopy (TEM) SIGMA 900 that is operated at an Accelerating Voltage of 80 kV are applied to observe their morphology. The chemical composition of the samples is determined by inductive coupled plasma atomic emission spectroscopy (ICP-AES). X-ray photoelectron spectroscopy (XPS, BES TEC, 8025) analysis is performed for investigation of oxidation state of transition metal.

2.3. Electrochemical measurements

In order to evaluate electrochemical performance of the NS-LMNCO sample, coin cells consisted of NS-LMNCO cathode are fabricated. For preparing cathode electrodes, the as-prepared NS-LMNCO active material, ultrapure graphite (Purity>99.99 wt. %) and PVDF (poly vinylidene fluoride, as a binder) are mixed in the weight ratio of 85:10:5, respectively. The electrode slurry is coated on a current collector, thin Al foil (10 μm). Afterwards, the electrode is dried in vacuum oven for 5 h in 70 ºC and pressed under controlled pressure. The coin cell is composed of the NS-LMNCO cathode, lithium metal anode, a polymer separator (celgard 2400) and electrolyte. The electrolyte solution is prepared by dissolving $LiPF_6$ salt in organic solvents e.g. ethylene carbonate (EC), dimethyl carbonate (DMC) and ethyl methyl carbonate (EMC). It should be noticed that the concentration of electrolyte is 1 M. Besides, the organic solvents are used in equal volume ratio (V:V:V=1:1:1).

Battery testing system (kimia stat-5 V/10 mA, kimia pardaz rayane, Iran) is used to investigate charge and discharge profiles of cathodes in the voltage range of 2.0- 4.8 V versus lithium at 25 ºC. Furthermore, the rate capability of NS-LMNCO electrode are investigated at different C-rates e.g. 0.1, 0.5, 2 and 5 C. The cyclic voltammetry (CV) analyses are conducted using a Galvanostat/Potentiostat Autolab (PGSTAT 302N). The excitation potential of 5 mV is applied. Besides, the minimum and maximum of applied frequencies are 10 mHz and 100 kHz, respectively.

3. RESULTS AND DISCUSSION

The XRD patterns of oxalate precursor and Li-rich oxide are shown in Fig. 1. Crystal structure of oxalate precursor well matched with LiC_2O_4, MnC_2O_4, CoC_2O_4 and NiC_2O_4. In fact, there is not any impurity in oxalate precursor.

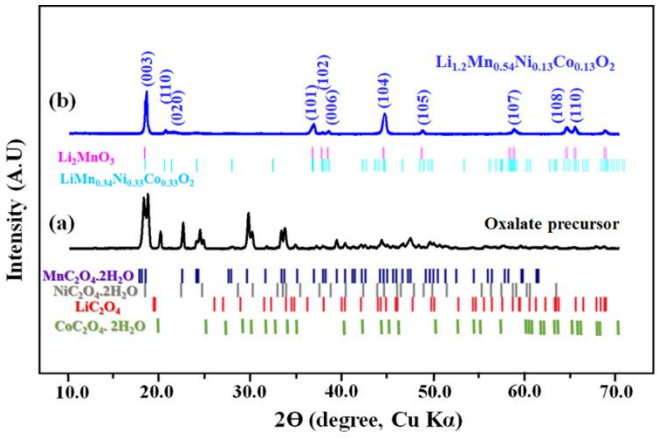

Fig. 1. XRD patterns of (a) oxalate precursor and (b) Nano sponge $Li_{1.2}Mn_{0.54}Ni_{0.13}Co_{0.13}O_2$ (NS-LMNCO)

Also, XRD pattern of NS-LMNCO sample clearly are composed of Li_2MnO_3 and $LiMn_{0.33}Ni_{0.33}Co_{0.33}O_2$ structures, resulting that layered-layered structure is successfully obtained. For NS-LMNCO sample, all peaks appear in the XRD patterns, expect weak peaks between 20^o and 25^o, attributed to the α-$NaFeO_2$ structure. The clear distinct splitting of (006)/ (102) and (108)/ (110) peaks for NS-LMNCO sample confirmed that this samples includes well-formed layered structure [18]. The NS-LMNCO sample shows good super-lattice structure appeared in the range of 20^o -25^o. The observable peaks are generally related to cation ordering between lithium and manganese ions in the monoclinic Li_2MnO_3 phase [19].

Additionally, the cation mixing of Nickel and lithium in the crystal structure of Li-rich particles is evaluated by dividing the intensity of (003) peak to (104) peak [7]. As can be observed in Table 1, this ratio of mentioned peak for NS-LMNCO sample is high, corresponding to that well mixed layered structure is obtained by synthesis method proposed in this work.

Besides, the elemental composition of NS-LMNCO sample are determined by inductively coupled plasma (ICP) analysis and shown in Table 1. This analysis confirmed that there is not any difference between experimental transition metal ratios and the theoretical composition of Li-rich cathode. Therefore, it can be concluded that the raw materials completely reacted in autoclave and during calcination step to obtain Li-rich product.

Table 1. ICP results for nano sponge $Li_{1.2}Mn_{0.54}Ni_{0.13}Co_{0.13}O_2$

Sample	Ni/Co	Mn/Co	Li / (Mn + Ni + Co)	I(003)/I(104)
NS-LMNCO	0.995	4.153	1.497	1.43

SEM images of oxalate precursor and NS-LMNCO are presented in Fig. 2. As can be observed in section a and a', the morphology of oxalate precursor includes Nano Plate particles with thickness of 60 nm and length of 2 µm. Section b and b' of Fig. 2 exhibits Nano Sponge like morphology for Li-rich oxide. It seems that the particles made sponge morphology include diameter of around 40 nm. It should be noticed that the Li-rich particles exhibited more porosity than oxalate precursor. Because the oxalate precursor converts to oxides by releasing carbon dioxide (CO_2) in the calcination step. As a result, the particles are separated and some pores are formed on the Li-rich oxide. More detailed morphological of oxalate precursor and NS-LMNCO sample are observed by TEM, as shown in Fig. 2 a" and b", respectively. The NS-LMNCO structure with high porosity and special morphology leads to the easy wetting of electrode particles with the liquid electrolyte. Finally, the electrochemical performance depended to high kinetics e.g. rate capability will be increased, corresponding to sufficient surface area for lithium ion intercalation and de-intercalation in layered structures of NS-

LMNCO cathode. The results show that ethanol has an effective role for designing specific morphology of Li-rich cathode.

In Fig 3a, b and c, the XPS measurement of NS-LMNCO for Mn, Ni and Co are presented, respectively. The Mn $2p_{3/2}$ and Mn $2p_{1/2}$ are appeared at 642 and 654 eV of Mn XPS spectrum, respectively, attributing to Mn^{4+}. The binding energies of the 780.0 and 795.9 eV are indicated Co^{3+}. Two peaks appeared at 855.6 and 873.3 eV in Ni XPS spectrum confirmed Ni^{2+} in structure of Li-rich cathode [20].

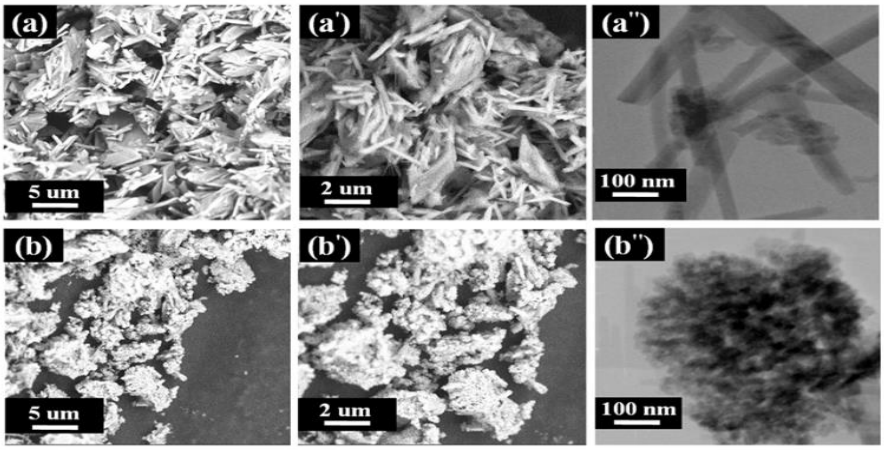

Fig. 2. FE-SEM and TEM micrographs of (a, a' and a'') oxalate precursor and (b, b' and b'') NS-LMNCO

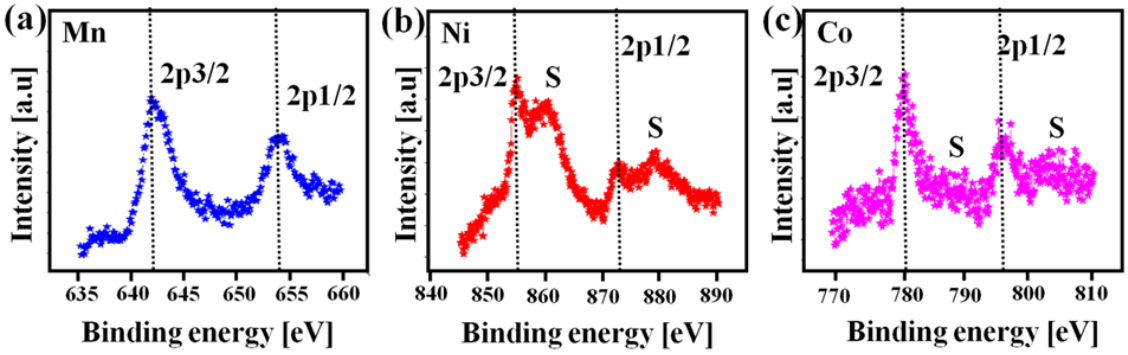

Fig. 3. X-ray photoelectron spectroscopy (XPS) of Mn (a), Ni (b) and Co (c) for NS-LMNCO

Cyclic voltammetry of NS-LMNCO is measured to investigate the electrochemical performances such as individual redox process in the voltage range of 2.0-4.8V at 0.1 mVs^{-1}. The voltammogram is shown in Fig. 4a for first, second, third and 10^{th} cycles. The NS-LMNCO sample exhibits two peaks during oxidation process at 4.5 and 4.6 V. The first one appeared at 4.5 V is related to redox couples of Ni^{2+}/Ni^{4+} and Co^{3+}/Co^{4+}. In other words, nickel and cobalt ions will be oxidized during lithium extraction of

$LiMO_2$ (M=Mn, Ni and Co). These electrochemical process appear as initial platform in charge profile, as shown with section (1) in Fig. 4b. Besides, extraction of lithium ions and oxygen to form lithium oxide from layered Li_2MnO_3 creates the second anodic peak can be seen at 4.6 V. It should be noticed that the layered Li_2MnO_3 will be activated at mentioned voltage range and made the second platform of the initial charge-discharge curve [21]. The details of mentioned mechanism are reported in the following equations [22]:

$$0.5Li_2MnO_3.0.5LiMn_{1/3}Ni_{1/3}Co_{1/3}O_2 \rightarrow 0.5Li_2MnO_3.Mn_{1/3}Ni_{1/3}Co_{1/3}O_2+0.5Li^+ +0.5e^- \quad (1)$$

$$0.5Li_2MnO_3.0.5LiMn_{1/3}Ni_{1/3}Co_{1/3}O_2 \rightarrow 0.5MnO_2.0.5Mn_{1/3}Ni_{1/3}Co_{1/3}O_2+0.5Li_2O \quad (2)$$

Two reduction peaks located at ~4.6–3.5 V on discharge process in the following cathodic sweep are related to Ni^{4+}/Ni^{2+} and Co^{4+}/Co^{3+}. Furthermore, the Mn^{4+} is also reduced in the process below 3.5 V [23].

The galvanostatic charge/discharge profiles of NS-LMNCO at initial, second, third and 10th cycles are shown in Fig. 4b between 2.0 and 4.8 V *vs* Li/Li^+ at 0.1 C. As mentioned before, the first plateaus at 4.0-4.3 V (section 1) represent the removal of lithium ions from the $LiNi_{1/3}Co_{1/3}Mn_{1/3}O_2$ component [24]. The second plateau which is long (section 2) exhibits the elimination of lithium oxide from Li_2MnO_3 making low initial coulombic efficiency in the first cycle of the Li-rich cathodes [25].

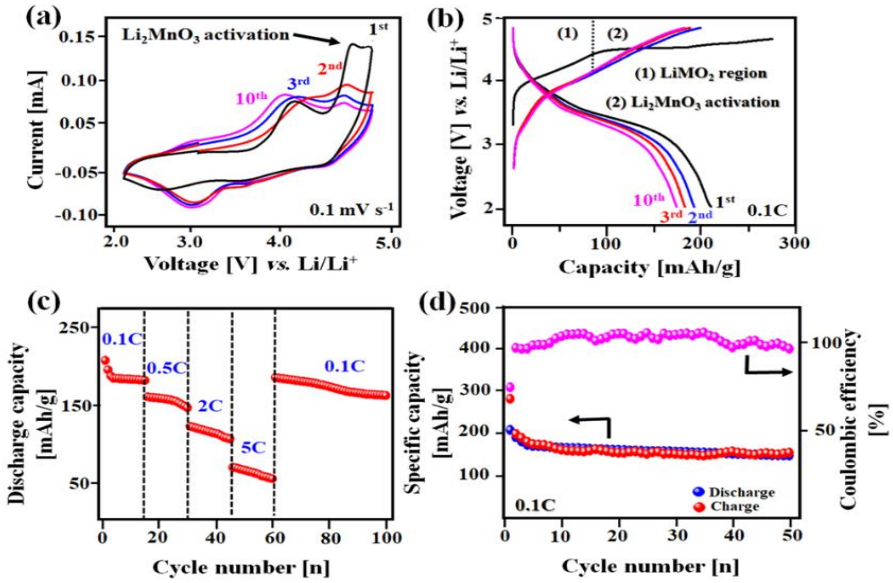

Fig. 4. (a) Cyclic voltammetry curves and (b) charge and discharge profiles of NS-LMNCO sample between 2 and 4.8 V recorded at a scan rate of 0.1 mV s^{-1} and 0.1 C, respectively. (c) Rate capacities of NS-LMNCO electrode at 0.1C to 5 C. (d) Cycling performance of NS-LMNCO at 0.1 C for 50 cycle

The initial charge and discharge capacities of NS-LMNCO are 280.5 and 207.6 mAh g^{-1}, respectively. It means that the initial coulombic efficiency of NS-LMNCO is 74%. The discharge capacities of NS-LMNCO for second, third and 10^{th} cycles are 190.6, 180.8 and 172.4 mAh g^{-1}, respectively.

Using LIBs for transportation applications highly depend to the rate performance and cycle stability of the cathode materials. The discharge capacity of NS-LMNCO sample are evaluated at 0.1, 1, 2 and 5 C for 15 cycles, respectively. In the final step, the capacities are measured for 40 cycles at 0.1 C. These results are presented in Fig. 4c. NS-LMNCO shows 207.6, 160.5, 122.8 and 70.5 mAh g^{-1} at 0.1, 1, 2 and 5 C, respectively. Therefore, it can be concluding that the NS-LMNCO sample with Nano Sponge morphology leads to improved kinetic rate. Moreover, the cycling performance of NS-LMNCO for 50 cycles are measured at lowest scan rate and presented in Fig. 4d. The discharge capacity of NS-LMNCO remains the value of 147.5 mAh g^{-1} at 0.1 C after 50 cycles with capacity retention of 71.1%. It is observed that the NS-LMNCO has the good capability for lithium ion movements during charge and discharge processes in lithium ion battery.

Electrochemical impedance spectrum (EIS) is used to evaluate the electrochemical performance of NS-LMNCO cathode in lithium ion battery. The Nyquist spectrum, linear relationship between real impedance and $\omega^{-1/2}$ and equivalent circuit of NS-LMNCO are exhibited in Fig. 4 a, b and c, respectively. The Nyquist spectra is consisted of one semicircle and quasi-straight line. The straight line at low frequency exhibits the Warburg impedance related to lithium ion diffusion in solid phase of the electrode materials. It is noteworthy to mention that other components of Li-ion cell e.g. electrolyte solution, wires and etc are created negligible resistance, as shown by R_e. The diameter of semicircle can be observed in the regions of high to medium frequencies is attributed to the charge-transfer resistance (R_{ct}). The values of the parameters (R_e and R_{ct}) are listed in Table 2. The R_{ct} for NS-LMNCO cathode is low, 274.32 Ω, which it is necessary to the high rate performance.

Besides, Li-ion diffusion coefficient (D_{Li+}) is usually obtained by slope determination of straight line in Warburg area. The following equation is used for this calculation process [26]:

$$D = R^2T^2/2A^2n^2F^4C^2\sigma^2 \quad (3)$$

Where R is 8.314 J K^{-1} mol^{-1}, T is 298 k, n is the number of electrons transferred per molecule during oxidization, F is 96,483.3 C mol^{-1}, A is the surface area of the electrode, and C is the concentration of Li ions and σ is the Warburg factor. The Warburg factor can be estimated by using equation mentioned below and drawing Fig 5b [26]:

$$Z_{re} = R_e + R_{ct} + \sigma\omega^{-1/2} \quad (4)$$

Where ω is the angular frequency appeared in the low frequency area.

The D_{Li+} is also reported in Table 2. The NS-LMNCO sample shows the fast lithium ion diffusion process during electrochemical reaction.

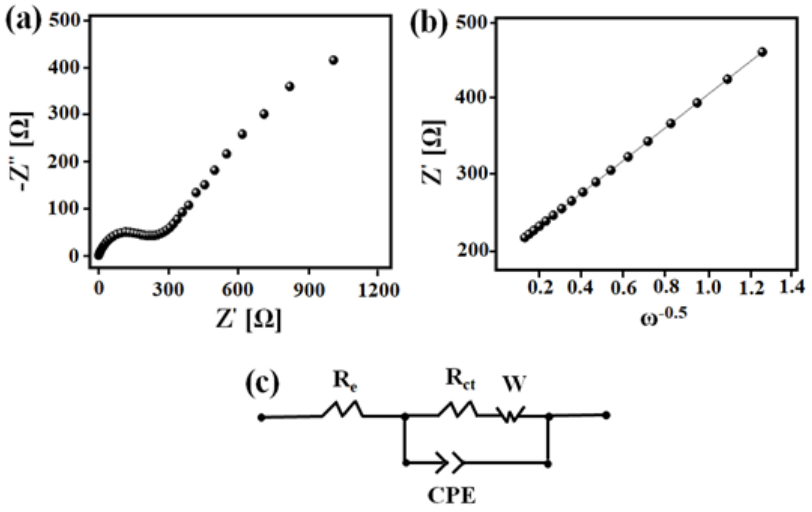

Fig. 5. (a) Nyquist plot, (b) Warburg factor determination plot of NS-LMNCO electrode at low frequencies and (c) equivalent circuit model. The double layer and passivation film capacitances are assigned by CPE

Table 2. The parameters obtained from EIS results for the Nano Sponge $Li_{1.2}Mn_{0.54}Ni_{0.13}Co_{0.13}O_2$

Sample	OCV(V)	R_e (Ω)	R_{ct} (Ω)	σ (Ω cm^2 s$^{-1/2}$)	D_{Li+} (cm^2 s^{-1})
NS-LMNCO	4.31	2.85	274.32	215.64	2.03×10^{-14}

4. CONCLUSION

In conclusion, the specific morphology of $Li_{1.2}Mn_{0.54}Ni_{0.13}Co_{0.13}O_2$ are synthesized with designing Nano plate oxalate precursor obtained by new procedure. The results showed that the ethanol significantly effects on designing the morphology of $Li_{1.2}Mn_{0.54}Ni_{0.13}Co_{0.13}O_2$ sample. The nano sponge $Li_{1.2}Mn_{0.54}Ni_{0.13}Co_{0.13}O_2$ (NS-LMNCO) exhibits good electrochemical performance in lithium ion battery. The reversible capacities are obtained 207.6 and 122.8 mA h g^{-1} at 0.1 and 2 C, respectively. Furthermore, this cathode shows discharge capacity of 147.5 mAh g^{-1} after 50 cycles. The good rate capability and cycle ability of NS-LMNCO are attributed to the special Nano Sponge morphology caused by nanoparticle size. The proposed synthesis method here prepares a new concept to obtain Li-rich cathode material with good structural and electrochemical properties.

Acknowledgements

The authors are grateful to Amirkabir University of Technology (Tehran, Iran) and Renewable Energy Research Center (RERC) for the technical support of this work.

REFERENCES

[1] V. Etacheri, R. Marom, R. Elazari, G. Salitra, D. Aurbach, Energy & Environmental Science, 4 (2011) 3243.

[2] K. Ozawa, Solid State Ionics, 69 (1994) 212.

[3] D.K. Kim, P. Muralidharan, H.-W. Lee, R. Ruffo, Y. Yang, C.K. Chan, H. Peng, R.A. Huggins, Y. Cui, Nano letters, 8 (2008) 3948.

[4] M. Rastgoo-Deylami, M. Javanbakht, M. Ghaemi, L. Naji, H. Midvar, M.R. Ganjali, Int. J. Electrochem. Sci, 9 (2014) 3199.

[5] M. Rastgoo-Deylami, M. Javanbakht, M. Ghaemi, H. Omidvar, H. Ghafarian, Anal. Bioanal. Electrochem., 5 (2013) 506.

[6] R. Jung, M. Metzger, F. Maglia, C. Stinner, H.A. Gasteiger, Journal of The Electrochemical Society, 164 (2017) A1361.

[7] D. Mohanty, S. Kalnaus, R.A. Meisner, K.J. Rhodes, J. Li, E.A. Payzant, D.L. Wood III, C. Daniel, Journal of Power Sources, 229 (2013) 239.

[8] X. Liu, J. Liu, T. Huang, A. Yu, Electrochimica Acta, 109 (2013) 52.

[9] L. Zhang, B. Wu, N. Li, D. Mu, C. Zhang, F. Wu, Journal of Power Sources, 240 (2013) 644.

[10] Z. He, Z. Wang, H. Chen, Z. Huang, X. Li, H. Guo, R. Wang, Journal of Power Sources, 299 (2015) 334.

[11] Y. Bai, Y. Li, C. Wu, J. Lu, H. Li, Z. Liu, Y. Zhong, S. Chen, C. Zhang, K. Amine, Energy Technology, 3 (2015) 843.

[12] S. Shi, J. Tu, Y. Tang, Y. Zhang, X. Wang, C. Gu, Journal of Power Sources, 240 (2013) 140.

[13] H. Ghafarian-Zahmatkesh, M. Javanbakht, M. Ghaemi, Journal of Power Sources, 284 (2015) 339.

[14] F. Fathollahi, M. Javanbakht, H. Omidvar, M. Ghaemi, Journal of Alloys and Compounds, 627 (2015) 146.

[15] F. Fathollahi, M. Javanbakht, H. Omidvar, M. Ghaemi, Journal of Alloys and Compounds, 643 (2015) 40.

[16] E. Golestani, M. Javanbakht, H. Ghafarian-Zahmatkesh, H. Beydaghi, M. Ghaemi, Electrochimica Acta, 259 (2018) 903.

[17] M. Rastgoo-Deylami, M. Javanbakht, H. Omidvar, Solid State Ionics, 331 (2019) 74.

[18] X. Miao, Y. Yan, C. Wang, L. Cui, J. Fang, G. Yang, Journal of Power Sources, 247 (2014) 219.
[19] Z. Zhu, L. Zhu, Journal of Power Sources, 256 (2014) 178.
[20] N. Yabuuchi, K. Yoshii, S.-T. Myung, I. Nakai, S. Komaba, Journal of the American Chemical Society, 133 (2011) 4404.
[21] S. Guo, H. Yu, P. Liu, X. Liu, M. Chen, M. Ishida, H. Zhou, Journal of Materials Chemistry A, 2 (2014) 4422.
[22] Y. Sun, Y. Zhou, L. Zhang, Y. Shen, J. Zeng, Journal of Alloys and Compounds, (2017).
[23] J. Zhang, Q. Lu, J. Fang, J. Wang, J. Yang, Y. NuLi, ACS applied materials & interfaces, 6 (2014) 17965.
[24] J.W. Min, A.K. Kalathil, C.J. Yim, W.B. Im, Materials Characterization, 92 (2014) 118.
[25] T.R. Penki, D. Shanmughasundaram, N. Munichandraiah, Electrochimica Acta, 143 (2014) 152.
[26] S. Yang, X. Wang, X. Yang, Y. Bai, Z. Liu, H. Shu, Q. Wei, Electrochimica Acta, 66 (2012) 88.